A Sequential Method to Prepare Polymorphs and Solvatomorphs of $[Fe(1,3bpp)_2](ClO_4)_2 \cdot nH_2O$ (n=0,1,2) with Varying Spin Crossover Behavior

C. Bartual-Murgui,*[a] C. Codina,[a] O. Roubeau*[b] and G. Aromí*[a]

Abstract: Two polymorphs of the spin crossover (SCO) compound $[Fe(1,3bpp)_2](ClO_4)_2$ (**1** and **2**; *1,3bpp,* 2-(pyrazol-1-yl)-6-(pyrazol-3-yl)-pyridine) are prepared using a novel, stepwise procedure. Crystals of **1** deposit from dry solvents while **2** is obtained from a solid-state procedure, by sequentially removing lattice H_2O molecules from the solvatomorph $[Fe(1,3bpp)_2](ClO_4)_2 \cdot 2H_2O$ (**2**$\cdot 2H_2O$), using single-crystal-to-single-crystal (SCSC) transformations. Hydrate **2**$\cdot 2H_2O$ is obtained through the same reaction as **1**, now with 2.5% of added water. Compounds **2** and **2**$\cdot 2H_2O$ are unstable in the atmosphere and absorb or lose one equivalent of water, respectively, to both yield the stable solvatomorph $[Fe(1,3bpp)_2](ClO_4)_2 \cdot H_2O$ (**2**$\cdot H_2O$), also following SCSC processes. The four derivatives have been characterized by single crystal X-ray diffraction (SCXRD). Furthermore, the homogeneity of the various compounds as well as their SCSC interconversions have been confirmed by powder X-ray diffraction (PXRD). Polymorphs **1**/**2** exhibit abrupt SCO near room temperature with $T_{1/2\uparrow}$ = 279/316 K and $T_{1/2\downarrow}$ = 276/314 K (near 40 K of shift) and different cooperativity.

Introduction

The phenomenon of spin crossover (SCO), exhibited by some octahedral d^4 to d^7 transition metals, continues to stimulate multidisciplinary research efforts worldwide as novel potential applications of this molecular property are envisaged.[1-3] The challenge of mastering this behaviour for its exploitation belongs largely to the realm of chemical design and synthesis. For example, ideal switching features rely on a good control of the cooperativity, which is mainly due to the elastic contacts between spin centers,[4] and governs the shape and width of a potential hysteresis effect during the spin transition (ST). On the other hand, the temperature of the transition is mainly dependent on the metal coordination sphere.[5] These properties can be modulated or fine-tuned through the good choice of the active metal, the ligands and the potentially accompanying counter ions. The solvents employed for the synthesis usually play a crucial role as well, since the presence of solvate molecules often affect dramatically the magnetic behaviour.[6-9] In this respect, the influence of water molecules has been especially studied.[10-12] More remarkably, some selected cases offer the opportunity to investigate the specific role of the crystallographic arrangement on the SCO while keeping all the above variables constant. It is the case of systems that are found as more than one polymorph.[13] The relatively few compounds that have been characterized as two or more polymorphs, also exhibiting SCO properties, have been recently reviewed.[14] The vast majority of them are obtained serendipitously, as mixtures of crystals. As a result, some of them cannot be accumulated in sufficient amount for bulk studies,[15] do not form systematically[16] or even, cannot be reproduced.[17] In one exceptional case, the sequential interconversion of polymorphs over long periods of time within the reaction system was described, presumably driven by the formation of systems of increasing thermodynamic stability.[18] Clearly, engineering alternative methods of preparing polymorphs, ideally involving a larger degree of rational design is highly challenging, but very desirable in this and other research areas.

Chemists have employed over the years many ligand sets for SCO research.[19-20] The family of 2,6-bis-(pyrazol-*x*-yl)-pyridine ligands (x=1 or 3 for 1bpp and 3bpp, Scheme I) and their derivatives is one of the most versatile in this respect, yielding countless systems of relevance to the field, especially with Fe(II),[21-23] which include cases of polymorphism.[24] This group of ligands are engaged in most of the scarce reported cases of single-crystal-to-single-crystal (SCSC) transformations of molecular systems resulting from exchange of lattice solvent molecules.[25-28] These processes, usually conducted near room temperature are often concomitant to spin transitions, which enhance the potential of such systems as chemo-sensors, since the change of composition is accompanied by drastic changes to the magnetic properties or to the colour.[25, 29] Molecular solids experiencing composition changes in SCSC manners are very interesting for single crystal X-ray diffraction (SCXRD) studies in real time of solid state transformations.[30]

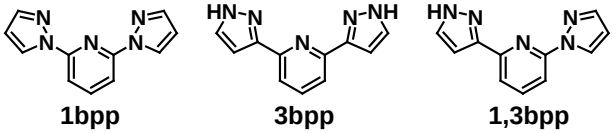

Scheme 1. Molecular structure of ligands 3bpp, 1bpp and 1,3bpp.

In this paper, we present a new rational method to produce separately polymorphs of SCO compounds, here using the relatively unexplored hybrid ligand 2-(pyrazol-1-yl)-6-(pyrazol-3-yl)-pyridine (1,3bpp; Scheme I).[31-34] Thus, the water free

[a] Dr. C. Bartual-Murgui, Mrs. C. Codina, Dr. G. Aromí
Departement de Inorgánica, Universitat de Barcelona, Diagonal 645, 08028, Barcelona, Spain. E-mail: carlos.bartual@qi.ub.es, guillem.aromi@qi.ub.es.
[b] Dr. O. Roubeau
Instituto de Ciencia de Materiales de Aragón (ICMA), CSIC and Universidad de Zaragoza, Plaza San Francisco s/n, 50009, Zaragoza, Spain.E-mail: roubeau@unizar.es.

polymorph $[Fe(1,3bpp)_2](ClO_4)_2$ (**1**) as obtained pure in high yield from dry solvents may be studied and analysed through SCXRD. Likewise, a bis-hydrate form of complex **1**, $[Fe(1,3bpp)_2](ClO_4)_2{\cdot}2H_2O$ (**2**$\cdot 2H_2O$), is obtained pure by using solvents with controlled amounts of added water. Interestingly, standing at room temperature or gently warming crystals of **2**$\cdot 2H_2O$ leads to the controlled evacuation of one molecule of H_2O, producing the stable monohydrate $[Fe(1,3bpp)_2](ClO_4)_2{\cdot}H_2O$ (**2**$\cdot H_2O$) in a SCSC manner, which allows studying the process through SCXRD. Heating **2**$\cdot H_2O$ further causes the evacuation of the remaining molecule of water, leaving behind the crystal lattice of the water free compound $[Fe(1,3bpp)_2](ClO_4)_2$ (**2**), which is a different polymorph of **1**, also amenable to SCXRD studies. The SCO properties of polymorphs **1** and **2** may be thus studied and their differing behaviour analysed in light of the structural features presented by each of them. The new stepwise method to produce SCO polymorphs should be of great benefit to this and other fields if it can be expanded to other related systems. In addition, the **2**$\cdot H_2O \rightarrow$ **2** transformation is reversible; in contrast to **1**, the water free phase **2** spontaneously absorbs one molecule of H_2O from the atmosphere at room temperature to return to the monohydrate form **2**$\cdot H_2O$ (Scheme II). No other system from the bpp/Fe(II) family had been studied by SCXRD at this level of detail in their various hydration levels, in particular as resulting from SCSC interconversions.

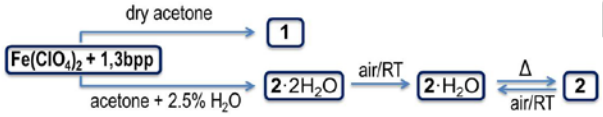

Scheme 2. Coordination chemistry transformations reported.

Results and Discussion

Synthesis and solvent exchange processes.

Complex $[Fe(1,3bpp)_2](ClO_4)_2$ (**1**) is obtained from stoichiometric amounts of its components as solvent free yellow crystals grown within the mixture of dry acetone (solvent) and dry diethyl ether (precipitating agent). If no precautions are taken to remove water from the solvents the reaction is not fully reproducible, with the occasional formation of orange crystals of another compound. The latter was established by SCXRD (*vide infra*) to be the bis-hydrate compound $[Fe(1,3bpp)_2](ClO_4)_2{\cdot}2H_2O$ (**2**$\cdot 2H_2O$). Thus, the reaction conditions need to be controlled carefully in order to access selectively either of both solvatomorphs. The use of dry solvents affords reproducibly pure anhydrous complex **1**, even in the presence of the water molecules from the Fe(II) salt. Increasing added amounts of water in the reaction solvent allow the preparation of complex **2**$\cdot 2H_2O$ reproducibly. Up to a 2% of added water produces mixtures of **1** and **2**. However, the range between 2% and 5% of water content leads to pure compound **2**$\cdot 2H_2O$ systematically. Above that percentage of water, no crystals form upon layering the reactions mixtures with diethyl ether. Compound **2**$\cdot 2H_2O$ is unstable in ambient conditions. SCXRD shows that in these conditions, the lattice loses one equivalent of water quite rapidly to transform into the stable new solvatomorph $[Fe(1,3bpp)_2](ClO_4)_2{\cdot}H_2O$ (**2**$\cdot H_2O$), while maintaining the crystallographic order. Furthermore, this new compound experiences full dehydration in a SCSC manner upon heating for 5 minutes at 350 K, yielding the new phase $[Fe(1,3bpp)_2](ClO_4)_2$ (**2**) while losing a second equivalent of water. Compound **2** is air-sensitive, therefore, it needs protection with oil before being brought to SCXRD experiments, which allow determining its structure. In fact, at room temperature it rapidly reabsorbs one equivalent of H_2O from the atmosphere to return to **2**$\cdot H_2O$ *via* a SCSC process as also shown through SCXRD. The structure of the monohydrated phase is independent of the way employed to reach it (absorption or extrusion of one equivalent of H_2O). All the solid state transformations described, *ie* **2**$\cdot 2H_2O \rightarrow$ **2**$\cdot H_2O \rightarrow$ **2** and **2** $\rightarrow$ **2**$\cdot H_2O$, are thus SCSC processes. Thus, water molecules may be removed sequentially in a controlled manner in order to form successively **2**$\cdot H_2O$ and **2**, while the stable **2**$\cdot H_2O$ form is a rare case where a monohydrate (**2**$\cdot H_2O$) may be accessed both, by water extrusion from a more hydrated derivative (**2**$\cdot 2H_2O$) or by moisture absorption from a drier solvatomorph (**2**). In sharp contrast with this, the polymorph of **2** obtained by direct synthesis, compound **1**, is stable in the atmosphere and does not accept spontaneously molecules of water into the lattice. The ability of preparing solvatomorphs **1** and **2**$\cdot 2H_2O$ in a controlled and repeatable manner opens the door of obtaining and characterizing two polymorphs of $[Fe(1,3bpp)_2](ClO_4)_2$, **1** and **2**, using a stepwise, fully reproducible procedure. The differing SCO properties of these two polymorphs can be studied in detail and correlated with the structure (see below).

Description of the Structures.

$[Fe(1,3bpp)_2](ClO_4)_2$ (1). Complex **1** crystallizes at room temperature from acetone/Et_2O as yellow crystals, which turn dark red at 100 K. At this temperature the lattice belongs to the monoclinic space group $P2_1/c$ (Table S1). The unit cell contains four asymmetric units, the composition of which coincides with the empirical formula (Fig. 1). The complex cation $[Fe(1,3bpp)_2]^{2+}$ features an Fe(II) centre chelated by two neutral, approximately planar 1,3bpp ligands providing a *mer* coordination environment. Both enantiomers of this species are present in the lattice, related by symmetry. The average of the Fe–N bond distances (1.952 Å; Table S4) indicates that at this temperature the compound is in the low spin (LS) state.[35] The ClO_4^- anions of this salt establish hydrogen bonds with the only two available N−H groups of the complex (Fig. 1, Table S2). This may have prevented the co-crystallization of solvent molecules that would accommodate within the lattice by establishing hydrogen bonds with other N−H fragments, if they had been available. The complex cations are disposed as sheets containing linear arrays (Figs. 2, top and S1). Within these arrays, all the complexes exhibit identical orientations, and are connected by π···π and C−H···π interactions. In between the chains, the complexes interact *via* additional, weaker C−H···π contacts, and alternate two orientations (dihedral angle between equivalent idealized ligands of adjacent complexes, 46.22°), as well as opposite chiralities. Thus, every $[Fe(1,3bpp)_2]^{2+}$ species

features six first neighbours within the sheets, two of which more strongly bonded than the other four (Fig. 2, top). The layers exhibit two different, alternative inter-layer separations (8.954 and 9.208 Å being the distances between the planes containing the metal atoms) where both crystallografically independent ClO_4^- anions are, respectively, located (Fig. S2). The latter mediate weak interactions between the sheets of complex cations *via* N–H···O and C–H···O contacts.

The structure of **1** was also determined at 296 K and 350 K on yellow crystals. In both cases, it is almost identical to that at 100 K, the main difference being the average of the Fe–N bond distances (2.141 and 2.157 Å for 296 and 350 K, respectively; Table S4), which shows, consistent with the colour change of the crystals, that the compound has experienced a SCO, now in the HS state in both cases. As a consequence of this transition, together with the thermal expansion, the unit cell volume experiences an essentially isotropic increase of 7 and 8 %, respectively (Table S1).

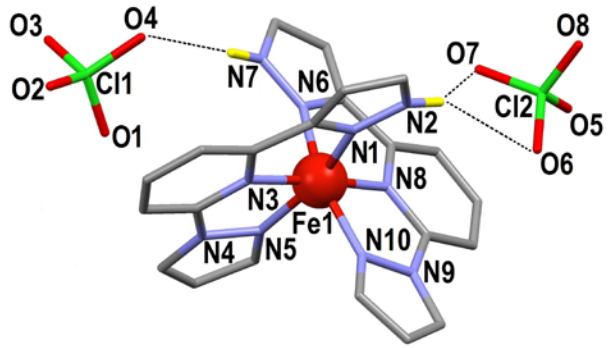

Figure 1. Molecular representation of $[Fe(1,3bpp)_2](ClO_4)_2$ (**1**) as determined at 100 K. Heteroatoms labelled. Only hydrogen atoms riding on N atoms shown (in yellow). Hydrogen bonds emphasized with dashed lines.

$[Fe(1,3bpp)_2](ClO_4)_2\cdot 2H_2O$ ($2\cdot 2H_2O$). The structure of compound $\mathbf{2}\cdot 2H_2O$ at 100 K, is monoclinic with the alternate settings of the space group of **1**, i.e. $P2_1/n$ (Table S1). Compared to **1** at the same temperature, the unit cell parameter *a* is now approximately half as long whereas the *c* parameter has nearly doubled. Thus, it still contains four asymmetric units, each with the composition $[Fe(1,3bpp)_2](ClO_4)_2$ in addition now to two water molecules. The presence of H_2O implies a 6.8 % increase of the unit cell volume, compared to **1** at the same temperature. The $[Fe(1,3bpp)_2]^{2+}$ cation of $\mathbf{2}\cdot 2H_2O$ is almost identical as in **1**, featuring average Fe–N bond distances of 1.943 Å, which confirms the LS state of the metal (Table S4). It is also present in both chiralities, although here distributed in alternative sheets, unlike for **1**. The main difference is that one of the original N–H···ClO_4^- hydrogen bonds has now been inserted by one molecule of H_2O, acting as donor towards the anion and as acceptor of the N–H proton, while in turn donating a proton to a second H_2O molecule (Fig. 3). In addition to the displacement of one ClO_4^- anion, the new structure exhibits the cross-shaped $[Fe(1,3bpp)_2]^{2+}$ cations in significantly different relative orientations compared to **1**, passing from lying 46.22° apart, to being all oriented the same (Fig. 2, bottom). Thus, the complexes are much more densely packed within the two dimensions defining the sheets (Fig. S3). Within these sheets, each complex is connected to four first neighbors *via* π···π and C−H···π interactions (Fig. 2, bottom), occupying more efficiently the surface containing the metals (1.40 *vs* 1.37 complexes/nm^2). The water molecules and the affected ClO_4^- species establish infinite arrays parallel to the *b* axis of repeating $[2H_2O, ClO_4^-]$ units in form of ribbons, where two types of fused rings of hydrogen bonded elements alternate; one engaging four H_2O molecules and two ClO_4^- anions and the other featuring two units of each species (Fig. 4A, Table S2). These ribbons are inserted within one of two different interlayer spaces separating the sheets of complexes, the layer-to-layer separations being now 9.098 and 10.819 Å, respectively (measured as the distances between planes containing the Fe centers). Thus, while both separations are larger with the presence of water, the space containing the inclusion molecules has become much wider than the other one (Δd of 1.61, and 0.14 Å, respectively, *ie* 17% *vs* 2%, Fig. 5). This increase of interlayer separation is responsible for the 6.8% volume increase seen when comparing **1** with $\mathbf{2}\cdot 2H_2O$, despite a more efficient organization of the $[Fe(1,3bpp)_2]^{2+}$ cations within the sheets. The interlayer space hosting the H_2O molecules appears to offer enough room for the ordered diffusion and evacuation of half of this water upon exposure to the atmosphere, leading to the formation of $\mathbf{2}\cdot H_2O$ *via* a SCSC process.

$[Fe(1,3bpp)_2](ClO_4)_2\cdot H_2O$ ($2\cdot H_2O$). The partially dehydrated compound $\mathbf{2}\cdot H_2O$ is obtained in SCSC manners through the controlled desorption of one water equivalent from $\mathbf{2}\cdot 2H_2O$, or through the absorption of water by the dehydrated derivative (see below). It is found in the space group $P2_1/n$. Its structure is very similar to that of the parent compound $\mathbf{2}\cdot 2H_2O$, with the same type of unit cell (Table S1) now containing half the amount of water molecules. This change has represented a slight shrinkage of the unit cell of 5% in volume. Here, the constituent $[Fe(1,3bpp)_2]^{2+}$ cations also bind directly one ClO_4^- anion *via* a N–H group and indirectly to another one through the intermediacy of one molecule of water (Fig S4). The average of the Fe–N bond distances at 100 K is 1.942 Å (Table S4), consistent with the LS state of the complex (*vide infra*). These cations maintain the two dimensional sheets organization of the parent compound (Figs. 2 and S5) with similar efficiency (1.39 complexes/nm^2). The molecules of H_2O remaining in $\mathbf{2}\cdot H_2O$ are connected to an N–H group of the complex cation and participate as proton donors within isolated [···$OClO_2O^-$···H–O–H···$OClO_2O^-$···H–O–H···] four-member cycles (Fig. 4B) lying next to each other as infinite arrays and filling the channels found parallel to the crystallographic *b* axis in between sheets of $[Fe(1,3bpp)_2]^{2+}$ complexes. These channels must be the pathway used by the molecules of water that evacuate and re-enter the lattice without collapsing it (see below). This lattice continues to differentiate two different interlayer spaces, one hosting the molecules of water and half of the ClO_4^- counter ions, and another containing the remainder of the ClO_4^- groups (Fig. S6). The interlayer separations are here 9.020 and 9.657 Å,

respectively, intermediate between these found for **1** and **2**·2H_2O, respectively.

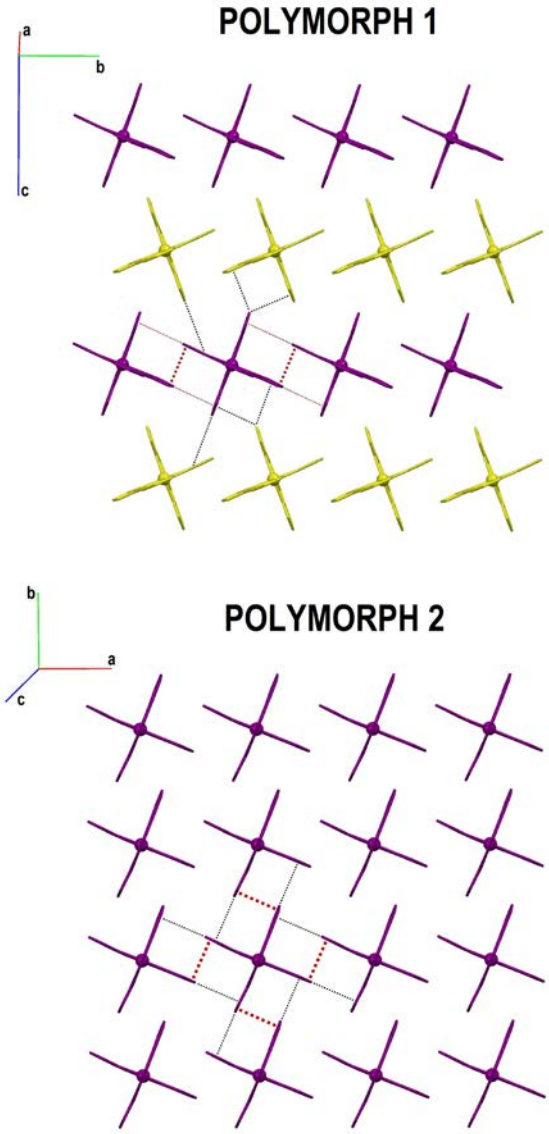

Figure 2. Organization within sheets of the $[Fe(1,3bpp)_2]^{2+}$ cations of **1** (top) and all the solvatomorphs of **2** (bottom), emphasizing the π···π (thick dashes) and C–H···π (thin dashes) interactions between one given complex and its six (for **1**) or four (for **2**) first neighbours.

$[Fe(1,3bpp)_2](ClO_4)_2$ (2). Compound **2** is the completely dehydrated version of **2**·2H_2O and **2**·H_2O. It is obtained as single crystals following the extrusion of water molecules from these solvatomorphs. The system is described by the monoclinic $P2_1/n$ space group, where the asymmetric unit coincides with its empirical formula. This compound is therefore a polymorph of **1**. The unit cell has the same composition as that of its solvatomorphs except that now it does not include any water. The cell volume is thus 6% smaller than in **2**·2H_2O (Table S1). The $[Fe(1,3bpp)_2]^{2+}$ cation of **2** is identical to that of the previous structures, now directly bound to two ClO_4^- anions, respectively, *via* its two available N–H groups (Fig. S7). The average of the Fe–N bond distances, 1.947 Å, reflects the LS of the Fe(II) centers at 100 K. The lattice is organized as sheets of complex cations as described for its hydrated congeners (Figs. 2 and S5). These sheets continue to show two different types of separation (Fig. S8). The narrow one (9.067 Å) lies in between these seen for the other solvatomorphs, although they oscillate within a very tight range with less than 1% variation. The larger interlayer space is the area presumably used by the H_2O molecules during their transit. In **2**, this separation is the smallest of the three solvatomorphs; 9.346 Å, 14% narrower that in **2**·2H_2O. This space is capable to readmit one molecule of water from the atmosphere producing **2**·H_2O, a process not possible for polymorph **1**. The specific mutual orientations of $[Fe(1,3bpp)_2]^{2+}$ complexes within the sheets of the lattice must be the key to explain this permeability difference.

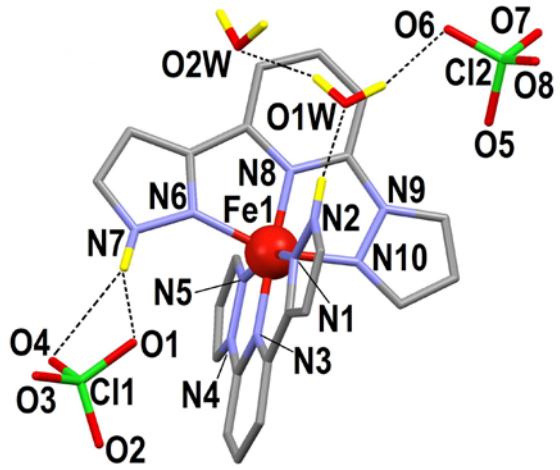

Figure 3. Molecular representation of $[Fe(1,3bpp)_2](ClO_4)_2$·2H_2O (**2**·2H_2O) at 100K. Heteroatoms labelled. Only hydrogen atoms riding N and O atoms shown (in yellow). Hydrogen bonds emphasized with dashed lines.

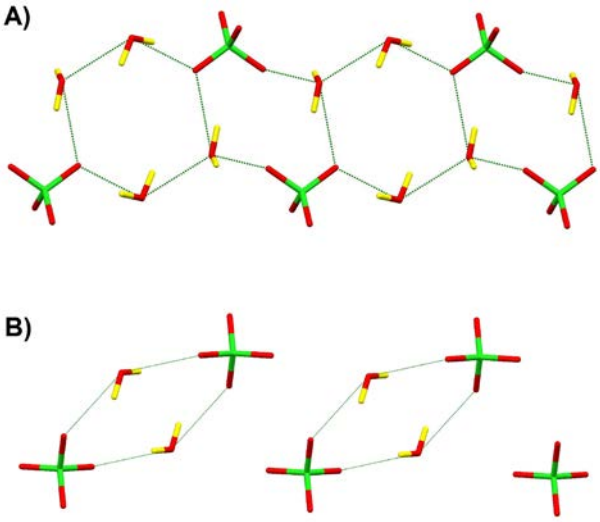

Figure 4. Representation of A) the repeating [2H_2O, ClO_4^-] units within **2**·2H_2O, forming ribbons of fused cycles cemented by hydrogen bonds (dashed lines) and B) the [2H_2O, 2ClO_4^-] independent cycles left in **2**·H_2O, after half of the molecules of water have left the lattice. Color code: red, O; green, Cl; yellow, H.

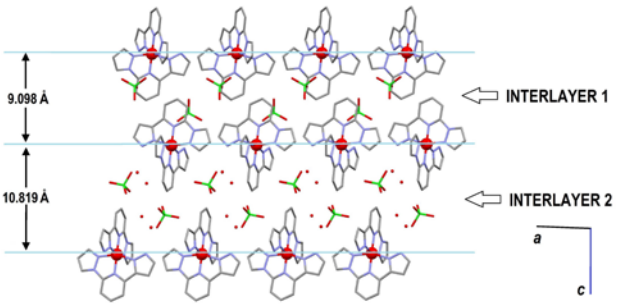

Figure 5. View of the lattice of $[Fe(1,3bpp)_2](ClO_4)_2 \cdot 2H_2O$ (**2**·2H$_2$O) along the sheets of cations (perpendicular to the *ac* crystallographic plane), emphasizing the two interlayer separations hosting or not, water molecules. Code: balls, Fe; red, O; green, Cl; grey, C. Hydrogen not shown.

Powder X-ray diffraction (PXRD).

The technique of PXRD is very useful to verify the identity and homogeneity in the bulk of the different phases characterized through SCXRD. Thus, compounds **1** and **2**·H$_2$O, which are stable at ambient conditions, were analyzed as synthesized and the resulting patterns are in good agreement with the simulated ones (Figs. 6 and S9). The pattern for **1** was compared with that simulated from the SCXRD structure obtained at 296 K, whereas for **2**·H$_2$O, the single crystal data obtained at 100 K were used. The non-perfectly random orientations of the polycrystalline samples and the temperature difference between the powder and the corresponding single crystal experiments explain the small discrepancies between experimental and simulated patterns. Compounds **2**·2H$_2$O and **2** are unstable in air, since the former loses water while the latter absorbs it. The PXRD of **2**·2H$_2$O was then measured immediately as synthesized, before starting to transform. Its experimental pattern is well reproduced from that produced from the SCXRD data (Figs. 6 and S9). Likewise, it is possible to form **2** *in situ* by heating to 390 K and obtaining the powder diffractogram while preventing water reabsorption (Figs. 6 and S9). At this temperature the compound is in the HS state (see below), whereas the only available structure of **2** was obtained at 100 K (in the LS state). The PXRD analysis of the protected sample was also performed at 200 K, where **2** is known to exist in the LS state (see below), and the comparison with the simulated pattern is satisfactory (Figs. 6 and S9). The method of PXRD was also used here to monitor the solid state transformations **2**·2H$_2$O → **2**·H$_2$O, **2**·H$_2$O → **2** and **2** → **2**·H$_2$O. Thus, compound **2**·2H$_2$O was examined at room temperature in air every 190 seconds. Diffractograms were recorded during this period, showing its gradual evolution into **2**·H$_2$O (Fig. S10). This evolution seems continuous, thus suggesting that no change of spin state occurs during the process, considering that both, the initial and the final systems are in the LS state at this temperature. Additionally, the thermal conversion from **2**·H$_2$O to **2** was followed by PXRD, by heating the stable monohydrate from 292 K to 373 K (Fig. S11). From the diffractograms, it seems like the water begins to evolve around 325 K and the transformation occurs then quite rapidly (see below). Since there is no evidence of any intermediate, the patterns suggest that **2**·H$_2$O remains in the LS state until it begins to lose water, converting into dehydrated **2** which itself is in the HS state at that temperature (in agreement with DSC observations using similar heating rates, see below). Finally, the water reabsorption by the latter from the atmosphere to convert anew into stable **2**·H$_2$O was followed. Compound **2** was brought to 298 K, thus converting to the LS state. It was then allowed to capture water from the atmosphere while the conversion to **2**·H$_2$O (also LS) was registered (Fig. S12). The transformation does occur in a continuous manner, without the apparent formation of any intermediate.

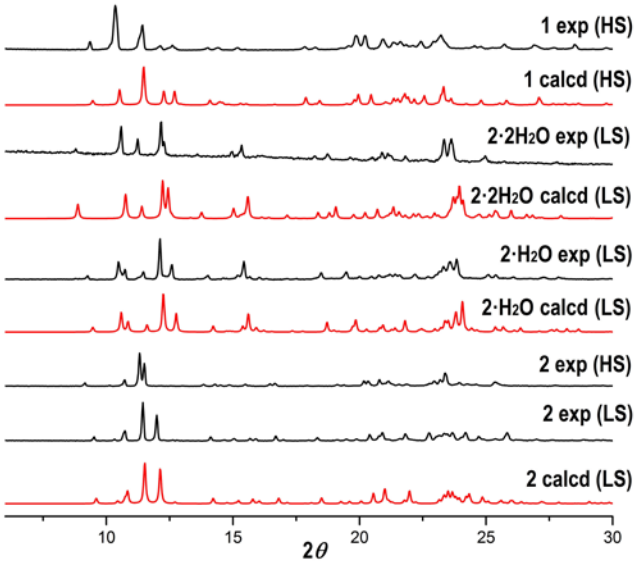

Figure 6. Experimental (black) PXRD diffractograms for compounds **1**, **2**·2H$_2$O, **2**·H$_2$O (300 K) and **2** (393 K and 200 K) and the corresponding simulated patterns (red) for these compounds obtained from the SCXRD data (see text). See Fig. S9 for a narrower angle range.

Thermogravimetric Analysis (TGA).

The technique of TGA is particularly useful for the study of the water exchange processes described above. Thus, a sample of **1** shows quasi no weight loss upon heating until nearly 170 °C, when decomposition is beginning to occur (Fig. S12). There is a very shallow step below 100 °C (≈373 K) corresponding to a weight loss of 0.3% of the mass that may be ascribed to superficial moist or residual solvent. By contrast, compound **2**·H$_2$O exhibits a sharp step centered near 50 °C (≈323 K) corresponding to the loss of one molecule of H$_2$O, thus to the **2**·H$_2$O → **2** transformation (Fig. S13). Interestingly, when a polycrystalline sample of **2**·H$_2$O was heated to 100 °C with the consequent loss of one molecule of H$_2$O, the original mass was recovered after the contact with the atmosphere. The thermal profile of the resulting product was very similar to that of **2**·H$_2$O (Fig. S12), thus confirming the reabsorption of the evacuated water upon contact of **2** with the atmosphere, during the course of a **2** → **2**·H$_2$O process. Further confirmation of this was obtained from DSC traces recorded for crystals of **2** after they had been exposed to air for one day (Fig. S14).

Magneto-Thermal Properties.

Since the lattice of **1** appears stable in the atmosphere, no special precautions were taken to determine its bulk magnetic properties. The variable temperature magnetic susceptibility of a

polycrystalline sample of **1** was determined under a constant magnetic field of 0.5 T. The $\chi_M T$ *vs.* *T* curve (χ_M is the molar paramagnetic susceptibility) reveals that complex **1** shows a relatively abrupt and complete SCO centred at *ca.* 278 K (Fig. 7 top), consistent with the colour changes observed on the crystals and with the X-ray diffraction experiments at 100, 296 and 350 K. A very narrow hysteresis opens in the steepest range of the transition, reaching 3 K at its widest point ($T_{1/2\uparrow}$ = 279 K and $T_{1/2\downarrow}$ = 276 K, Fig. S15). Confirmation of this behaviour is obtained from Differential Scanning Calorimetry (DSC). Indeed the DSC trace exhibits a broad endothermic/exothermic anomaly upon warming/cooling, culminating at 279.5/275.5 K (Fig. S16). The existence of a small but real hysteresis is supported by the fact that its width derived from DSC data, performed at 10 K/min, almost coincides with that derived from magnetic measurements, done in a settle mode at an average rate of 0.1 K/min. The molar heat capacity of **1** is thus dominated by a broad peak assigned to the SCO process (Fig. 7 bottom). A very small hump is observed at slightly higher temperatures, which is not detected with the magnetic measurements. It can be reasonably associated to a minute impurity of **2** in the measured sample, since it coincides with the sharper peak observed for this polymorph (see below).

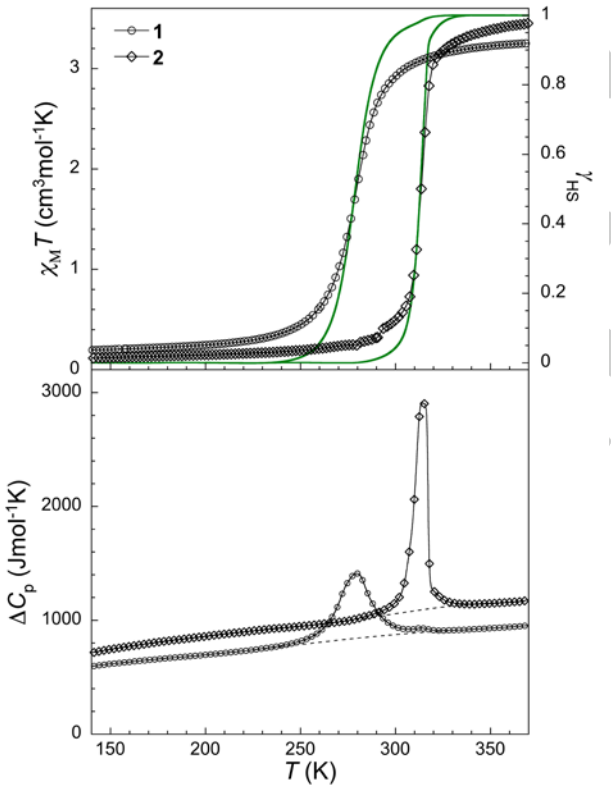

Figure 7. Thermal SCO properties of compounds **1** and **2**: $\chi_M T$ *vs.* *T* plots (top) and molar heat capacity at constant pressure as derived from DSC measurements (bottom). The full green lines (top) depict the HS fraction obtained from the latter as $\Delta H(T)/\Delta H_{sco}$, while the dashed lines (bottom) are the estimated lattice heat capacity. All data shown correspond to the warming mode.

Although compound **2** is not stable towards re-absorption of moist from ambient air, its magneto-thermal properties can be recorded after warming **2·H$_2$O** above 350 K for a few minutes. This can be done either ex-situ (avoiding the contact with air before the measurements) or inside the instrument of measurement. The resulting magneto-thermal characterization is for both cases virtually identical (Fig. S18). Complex **2** exhibits a complete SCO at *ca.* 315 K (Fig. 7), reproducible over successive warming and cooling cycles, and more abrupt than that of its polymorph **1**. The $\chi_M T$ *vs.* *T* curve indicates again the presence of a narrow hysteresis with $T_{1/2\uparrow}$ = 316 K and $T_{1/2\downarrow}$ = 314 K (Fig. S17). This is mirrored by the $C_p(T)$ curve that shows a sharp anomaly in the same temperature range ascribed to the SCO process. The excess heat capacities associated with the SCO of **1** and **2** (Fig. S19) were derived from the corresponding C_p data (Fig. 7 bottom), using lattice contributions estimated from the data below and above the SCO anomaly. Integration over *T* and Ln*T* then provides SCO enthalpy and entropy excesses of ΔH_{sco} = 13.57/17.74 kJmol^{-1} and ΔS_{sco} = 48.7/56.8 Jmol^{-1}K, respectively, in the **1**/**2** format. For both compounds, the relatively large calorimetric figures derived are an indication of cooperativity, more significant for polymorph **2**. In particular, the excess entropy is more than 3-4 times the electronic component, *R*ln5, pointing at a significant coupling of the electronic transition with lattice phonons.[36] The thermal dependence of the HS fraction derived from these calorimetric data as $\Delta H(T)/\Delta H_{sco}$ is in excellent agreement with the magnetic data for both compounds (full green lines in Fig 7 top).

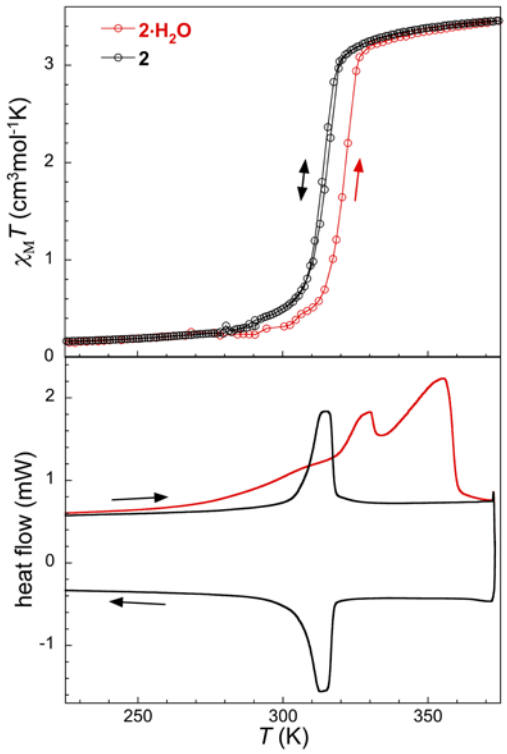

Figure 8. Magnetic and calorimetric characterization of compound **2·H$_2$O** depicting the SCO properties of **2·H$_2$O**, the **2·H$_2$O** → **2** transformation and the subsequent properties typical of **2**: $\chi_M T$ *vs.* *T* plot (top) and DSC traces

(bottom). The first warming scan is shown in red and subsequent reproducible cycle in black, as indicated.

The so-called domain model was used to quantify the degree of cooperativity in the SCO of polymorphs **1** and **2,** apparently higher in the latter as indicated by larger thermodynamic figures, compared to **1**. It uses calorimetric figures of the transition and a number *n* of like-spin SCO centres within an interacting domain, the higher the value of *n*, the more cooperative the transition.[37] Values for *n* of 10 to up to 95 have been reported for cooperative SCO systems,[38-40] while values close to unity correspond to gradual solution-like behaviour.[41-42] Here the excess heat capacity data are very nicely reproduced by this model (red lines in Figure S19) with n(**1**) = 8.5(1)/$T_{1/2\uparrow}$(**1**) = 278.8(3) K and n(**2**) = 20.0(2)/$T_{1/2\uparrow}$(**2**) = 313.4(3) K for **1** and **2**, respectively, indicating a 2-fold increase in cooperative character from one polymorph to the other. The latter can be associated with the expected effect of an increased efficiency of the intermolecular interactions (π···π and C–H···π) between $[Fe(1,3bpp)_2]^{2+}$ cations within the two dimensional sheets (Table S3, Fig. 2, see below). On the other hand, the stabilization of the LS state seen in **2** may be related to stronger N–H···$OClO_3^-$ bonds compared to **1** (Table S2). The effect on the Fe(II) spin state caused by the presence of lattice H_2O in the corresponding bis- and mono-hydrates **2**·2H_2O and **2**·H_2O was also investigated. This could however only be done with confidence for the latter, due to the ease with which the transformation **2**·2H_2O → **2**·H_2O takes place. Thus, the $\chi_M T$ *vs. T* plot of the stable **2**·H_2O shows a SCO process, similar to that of its anhydrous congener **2**, but shifted by *ca.* 7 K towards higher temperatures ($T_{1/2\uparrow}$ = 322 K, Fig. 8 top). Upon cooling, the solid returns to the LS state ($T_{1/2\downarrow}$ = 314 K) in the exact same manner as seen for **2**. The LS → HS transition may be ascribed to thermal SCO of **2**·H_2O, to the dehydration process **2**·H_2O (LS) → **2** (HS), or to both at the same time. Attempts to elucidate this were carried out through DSC measurements. At fast rate (10 K min^{-1}), the trace of **2**·H_2O (Fig. 8 bottom) features a large and asymmetric process beginning very gradually around 300 K, becoming very energetic above 340 K and ending abruptly around 360 K. Superimposed to this peculiar feature, a sharper anomaly is seen in the region 318-334 K. Subsequent cooling and heating cycles only reproduce the behaviour of **2**. Thus, the original trace can be interpreted as the loss of water of the **2**·H_2O → **2** process observed over a large temperature range (due to the fast warming rate) superimposed to the thermal SCO of **2**·H_2O starting at 318 K. Thus, in these conditions most of the water removal takes place after **2**·H_2O has transformed to the HS state. On the other hand, DSC traces show that slowly warming **2**·H_2O (1 Kmin^{-1}) and only up to 323 K, and keeping this temperature for near three hours allows to recover the typical thermal behaviour of **2** (Fig. S20).[‡] This confirms that the dehydration can be achieved entirely from **2**·H_2O in its LS state (<323 K) if the temperature is raised slowly, in agreement with temperature-dependent PXRD. The same experiment on fresh crystals of **2**·2H_2O results in identical DSC traces, confirming that the first dehydration **2**·2H_2O → **2**·H_2O readily occurs under the used conditions (Fig. S20). All the above shows that the lattice water extrusion from **2**·H_2O is not coupled to the SCO process of this material, and suggest that the LS → HS transition seen on the $\chi_M T$ *vs. T* curve and the sharper DSC peak recorded in the fast warming mode, both centred at *ca.* 322 K, correspond to the SCO of **2**·H_2O.

The stabilization of the LS state observed for the mono-hydrated version of **2** (by *ca.* 7 K, Fig. 8) is consistent with previous reports on other Fe(II) complexes with 3bpp-like ligands.[12, 43] Clearly, this is related to the effect that components outside the first coordination sphere have on the crystal field around the metal ion, here *via* the strength and efficiency of the hydrogen bonds to the N–H groups of the 1,3bpp ligands. In the present case, stronger interactions involving lattice neutral water molecules instead of the anionic perchlorate counter anion (Table S2) appear to stabilize the LS state. However, this has not always been the case,[44] showing that such aspects are sensitive to many parameters and difficult to rationalize.[6, 45-46]

Magnetostructural studies

The differences in SCO behaviour between **1** and **2** are strictly related to the intermolecular interactions operating within each of the lattices. These features may be analysed by means of Hirshfeld surfaces (Fig. 9).[47] For a given species, this surface encloses the space where the electron density of this species dominates over that from the reminder of the crystal. Each point of the surface is characterized by two coordinates (d_i,d_e) where d_i and d_e are the distance from that point to the closest atom inside and outside this surface, respectively. A normalized distance (d_n) for each point, which considers the sum of van der Waals (VdW) radii is shown on the surface with a colour code; red, white and blue for interactions shorter, equal or longer than VdW contacts.[48] The distribution of (d_i,d_e) points featured by a given surface is summarized in a fingerprint plot, with blue colour for less frequent occurrences and green for higher densities.[49] The Hirschfeld surfaces of compounds **1** and **2** (Fig. 9) show intense red circles for the N–H···O hydrogen bonds corresponding to the interaction with the ClO_4^- anions (Table S2). The C–H···π and π···π interactions are evident on the surface by the white colours in the middle of the concerned aromatic rings. These are more marked on the surface of **2** than for **1** (Fig. 9). The prominence of C–H···π interactions in polymorph **2** is also visible with marked features on the sides of the fingerprint plots (Fig. 9), and most especially with the more intense areas of π···π interactions. This analysis is consistent with the more abrupt nature of the SCO of polymorph **2** compared to **1** (see above), which is a reflect of the better packing of the $[Fe(1,3bpp)_2]^{2+}$ cations in the former. As mentioned before, the stabilization of the LS in **2** by 40 K is probably most related with stronger N–H···O hydrogen bonds between the perchlorate anions and the complex cation, also resulting from differences in the crystal lattice between both polymorphs.

Conclusions

The careful control of water content in the reaction solvent allows preparing selectively either of two, $[Fe(1,3bpp)_2](ClO_4)_2$ (**1**) or $[Fe(1,3bpp)_2](ClO_4)_2$·2H_2O (**2**·2H_2O) analogues. The latter

readily loses one equivalent of water thus generating the stable mono-hydrate solvatomorph $[Fe(1,3bpp)_2](ClO_4)_2 \cdot H_2O$ (**2**·H_2O).

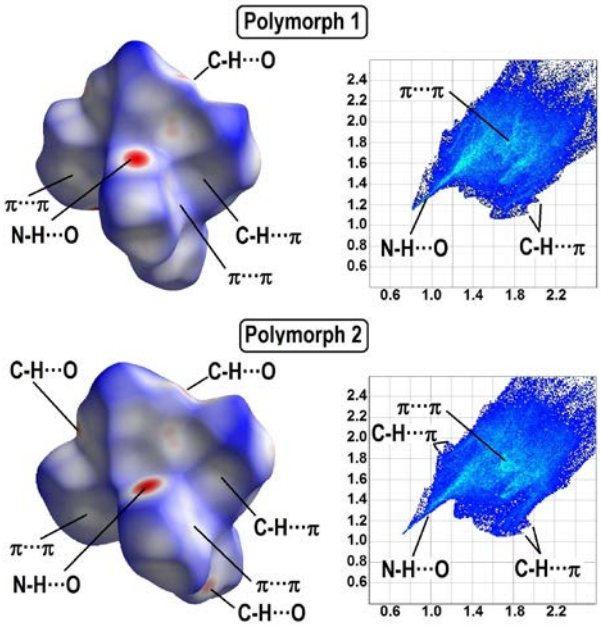

Figure 9. (left) Hirshfeld surfaces of the $[Fe(1,3bpp)_2]^{2+}$ cation of polymorphs **1** (top) and **2** (bottom), emphasizing the intense N–H···O hydrogen interaction and the importance of the CH···π and π···π contacts, and (right) fingerprint plots of these surfaces, where the relevant interatomic interactions are indicated (see text).

Gentle heating then allows the formation of a polymorph of anhydrous **1**, $[Fe(1,3bpp)_2](ClO_4)_2$ (**2**). This later process is reversed upon exposure of **2** to the atmosphere at room temperature. Remarkably, all these transformations take place in a SCSC manner. The location of all the molecules of water, along parallel channels formed by perchlorate anions between compact sheets of $[Fe(1,3bpp)_2]^{2+}$ cations suggests a pathway for ordered diffusion of H_2O in or out the lattice, with persistence of the crystallinity. On the other hand, polymorph **1** is stable and does not absorb H_2O from the atmosphere. These remarkable properties have served to discover an original and controlled method for preparing different polymorphs of a SCO molecular coordination network. SCO polymorphs are of great interest to establish the correlation between cooperativity and the crystal lattice. This new way of preparing polymorphs shall open the door of studying many more systems if they are amenable to controlled solvent extrusion. In this particular case, the more efficient crystal packing in polymorph **2**, associated with better intermolecular interactions (π···π and C–H···π) results in an increase of the cooperativity. Stronger N–H···O bonds involving the ClO_4^- anions in the latter polymorph are the likely cause of the increase in SCO temperature of the $[Fe(1,3bpp)_2](ClO_4)_2$ species by nearly 40 K from $T_{1/2\uparrow}$ = 278 K. On the other hand, chemical control of the reaction together with ordered extrusion of water with persistence of the crystal organization allows for a description of the magnetic properties of three solvatomorphs in light of accurate structural details, rarely seen in a family of $[Fe(bpp)_2]^{2+}$ complexes.

Experimental Section

Synthesis.

Ligand 2-(pyrazol-1-yl)-6-(pyrazol-3-yl)-pyridine (1,3bpp) was prepared by a slight modification (see SI) of a published procedure.[31] The requirements of dry solvents were fulfilled with Aldrich HPLC grade acetone of >99.8% purity and Aldrich anhydrous Et_2O of >99.7% purity. **Caution:** Perchlorate salts of metal complexes are potentially explosive. Only small quantities of material should be prepared and the samples should be handled with care.

$[Fe(1,3bpp)_2](ClO_4)_2$ (1). A solution of 1,3bpp (0.025 g, 0.12 mmol) in dry acetone (10 mL) was added dropwise with stirring to a solution of $Fe(ClO_4)_2 \cdot 6H_2O$ (0.023 g, 0.065 mmol) and ascorbic acid (~2 mg) in dry acetone (10 mL). The resulting orange solution was stirred for 30 min at room temperature, before being filtered and layered with dry diethyl-ether (volume 1:1). Yellow crystals suitable for X-ray diffraction formed after 2 days. The yield was 48%. EA, calcd (%) for $C_{22}H_{18}Cl_2FeN_{10}O_8$, **1** (found): C, 39.02 (39.15); H, 2.68 (2.46); N, 20.68 (20.41).

$[Fe(1,3bpp)_2](ClO_4)_2 \cdot 2H_2O$ (2·2H_2O). The previous reaction was performed using acetone with 2.5% of added water. Here, diethyl ether (40 mL) was poured onto the reaction mixture and the ensemble was mixed, leading to an orange suspension. After one hour, dark orange crystals of pure compound **2**·2H_2O were deposited, leaving behind a pale yellow solution. The yield was 40%.

$[Fe(1,3bpp)_2](ClO_4)_2$ (2). Crystals of **2**·2H_2O were heated in an oven for 5 minutes at 350 K. The resulting light orange crystals have to be kept isolated from the atmosphere since they react fast with ambient moisture. In order to perform SCXRD studies, the crystals were immersed in oil and rapidly cooled to 100 K. The experiment revealed the identity of the new compound as anhydrous **2**.

$[Fe(1,3bpp)_2](ClO_4)_2 \cdot H_2O$ (2·H_2O). *Method 1*. Crystals of **2** were left in the atmosphere for 30 minutes. Dark orange crystals were recovered while the crystalline integrity was maintained. The identity of this compound, stable in the atmosphere at room temperature was established by SCXRD (at 296 K) and PXRD. EA, calcd (%) for $C_{22}H_{20}Cl_2FeN_{10}O_9$, **2**·$H_2O$ (found): C, 38.01 (37.49); H, 2.90 (2.76); N, 20.15 (19.63).

Method 2. Crystals of **2**·2H_2O were left in the atmosphere for about one hour. During this period no apparent colour change takes place. However, SCXRD (obtained at 100 K) as well as PXRD certify that full conversion to **2**·2H_2O has taken place after this time. The structural details of **2**·H_2O are the same, regardless of the solid state procedure employed to obtain it.

Physical Measurements.

Elemental analyses were performed at the Scientific and Technological Centers of the University of Barcelona using an elemental organic analyser Thermo EA Flash 200 working in recommended standard conditions.

Magnetic measurements were performed with a Quantum Design MPMS5 SQUID magnetometer at the "Unitat de mesures Magnètiques" of the Universitat de Barcelona. Diamagnetic corrections for the sample holder were applied as well as a correction for the diamagnetic contribution of the sample, as derived from Pascal's constants.

Thermogravimetric Analysis (TGA). Experiments were performed using a Mettler-Toledo TGA-851e thermos-balance. Samples were introduced in alumina crucibles of 70 mL volume and heated at 10 K/min from room temperature to 230ºC under a dry nitrogen atmosphere.

Differential Scanning Calorimetry (DSC) experiments were carried out using a Q1000 calorimeter from TA Instruments equipped with the LNCS accessory. The temperature and enthalpy scales were calibrated with a standard sample of In, using its melting transition (156.6 °C, 3296 $Jmol^{-1}$). The measurements were carried out using Al pans with an empty pan as a reference at a scanning rate of 10 $Kmin^{-1}$. The pans were crimped mechanically, not representing a hermetic sealing, and therefore allowing the escape of gases. Open pans were also used in order to obtain better details on the processes of water extrusion. For heat capacity, a synthetic sapphire was measured in the same temperature range. By comparison, an overall accuracy of 0.2 K for the temperature and up to 10% for the heat capacity was estimated over the whole studied temperature range.

Powder X-ray Diffraction (PXRD). Patterns for **1** were recorded through the Servicio General de Apoyo a la Investigación-SAI, Universidad de Zaragoza, using a D-Max Rigaku diffractometer equipped with a Cu rotating anode and graphite monochromator to select the Cu $Ka_{1,2}$ wavelength, with 2θ ranging from 3 to 60° at a step size of 0.03°. The remaining samples were measured on a PANalytical X'Pert PROMPD diffractometer in transmission configuration using Cu Kα1+2radiation (λ= 1.5406 Å) with a focalizing elliptic mirror and a PIXcel detector working at a maximum detector's active length of 3.347°. The time evolution of the dehydration of **2**·$2H_2O$ to yield **2**·H_2O was followed at room temperature using a flat geometry with **2**·$2H_2O$ sandwiched between low absorbing films (polyester of 3.6 μm of thickness) measuring from 2 to 50° in 2θ with a step size of 0.026° registering successive scans every 190 s. The thermal evolution of **2**·H_2O was studied by placing the sample in a glass capillary (Lindemman) of 0.5 mm of diameter and measuring from 2 to 50° in 2θ, with a step size of 0.026°. One side of the capillary was open in order to allow the release of water molecules from the crystal lattice. The temperature of the sample was modified through a N_2 stream around the capillary controlled with an Oxford Cryostream equipment. Scans every 30 minutes were performed while the temperature was increased. Two scans were performed at 295, 325, 355, 275, and 200 K, whereas 6 and 5 scans with 30 minutes of time separation were acquired at 395 K and 295 K, respectively. The H_2O reabsorption process (**2** → **2**·H_2O) in the atmosphere was monitored by registering successive scans every 30 minutes at room temperature on the dehydrated sample in the absence of a nitrogen stream and, consequently, allowing the entry of moist air into the open capillary.

Single Crystal X-ray Diffraction (SCXRD). Data were collected on a Bruker APEXII QUAZAR diffractometer equipped with a microfocus multilayer monochromator with MoKα radiation (λ = 0.71073Å). Data reduction and absorption corrections were performed with SAINT and SADABS,[50] respectively. All structures were solved by intrinsic phasing with SHELXT[51] and refined by full-matrix least-squares on F^2 with SHELXL-2014.[52] All details can be found in CCDC 1427194-1427196 (**1**-100 K, **1**-296 K, **2**·$2H_2O$-100 K), 1438995-1438996 (**1**-350 K, **2**·H_2O-100 K), 1473474 (**2**·H_2O-292 K) and 1473454 (**2**-100 K) that contain the supplementary crystallographic data for this paper. These data can be obtained free of charge from The Cambridge Crystallographic Data Center via https://summary.ccdc.cam.ac.uk/structure-summary-form. Crystallographic and refinement parameters are summarized in Table S1. Selected bond lengths and angles and intermolecular distances are given in Tables S2 to S4.

Acknowledgements

The authors thank the Generalitat de Catalunya for the prize ICREA Academia 2008 and 2013, the ERC for Starting Grant StG-2010-258060 (GA) and MINECO through MAT2014-53961-R and MAT2015-70868-ERC (OR) and CTQ2012-32247 and CTQ2015-68370-P (GA, CBM).

Keywords: Polymorphism • Spin Crossover • Single-crystal-to-single-Crystal • Fe(II) • Solvatomorph

[1] M. A. Halcrow, *Spin-Crossover Materials: Properties and Applications*, John Wiley & Sons Ltd, **2013**.
[2] A. Bousseksou, G. Molnar, L. Salmon, W. Nicolazzi, *Chem. Soc. Rev.* **2011**, *40*, 3313-3335.
[3] P. Gamez, J. S. Costa, M. Quesada, G. Aromi, *Dalton Trans.* **2009**, 7845-7853.
[4] H. Spiering, *Top. Curr. Chem.* **2004**, *235*, 171-195.
[5] A. Hauser, in *Spin Crossover in Transition Metal Compounds I, Vol. 233* (Eds.: P. Gütlich, H. A. Goodwin), Springer Berlin Heidelberg, **2004**, pp. 49-58.
[6] G. A. Craig, J. Sanchez Costa, O. Roubeau, S. J. Teat, G. Aromi, *Chem., Eur. J.* **2012**, *18*, 11703-11715.
[7] S. Bonnet, G. Molnar, J. S. Costa, M. A. Siegler, A. L. Spek, A. Bousseksou, W.-T. Fu, P. Gamez, J. Reedijk, *Chem. Mater.* **2009**, *21*, 1123-1136.
[8] R.-J. Wei, J. Tao, R.-B. Huang, L.-S. Zheng, *Inorg. Chem.* **2011**, *50*, 8553-8564.
[9] W. Zhang, F. Zhao, T. Liu, M. Yuan, Z.-M. Wang, S. Gao, *Inorg. Chem.* **2007**, *46*, 2541-2555.
[10] K. Sugiyarto, D. Craig, A. Rae, H. Goodwin, *Aust. J. Chem.* **1994**, *47*, 869-890.
[11] T. D. Roberts, M. A. Little, F. Tuna, C. A. Kilner, M. A. Halcrow, *Chem. Commun.* **2013**, *49*, 6280-6282.
[12] T. D. Roberts, F. Tuna, T. L. Malkin, C. A. Kilner, M. A. Halcrow, *Chem. Sci.* **2012**, *3*, 349-354.
[13] A. J. Cruz-Cabeza, S. M. Reutzel-Edens, J. Bernstein, *Chem. Soc. Rev.* **2015**, *44*, 8619-8635.
[14] J. Tao, R.-J. Wei, R.-B. Huang, L.-S. Zheng, *Chem. Soc. Rev.* **2012**, *41*, 703-737.
[15] S. M. Neville, B. A. Leita, D. A. Offermann, M. B. Duriska, B. Moubaraki, K. W. Chapman, G. J. Halder, K. S. Murray, *Eur. J. Inorg. Chem.* **2007**, *2007*, 1073-1085.
[16] G. S. Matouzenko, A. Bousseksou, S. Lecocq, P. J. van Koningsbruggen, M. Perrin, O. Kahn, A. Collet, *Inorg. Chem.* **1997**, *36*, 5869-5879.
[17] C. Faulmann, P. A. Szilagyi, K. Jacob, J. Chahine, L. Valade, *New J. Chem.* **2009**, *33*, 1268-1276.
[18] R.-J. Wei, B. Li, J. Tao, R.-B. Huang, L.-S. Zheng, Z. Zheng, *Inorg. Chem.* **2011**, *50*, 1170-1172.
[19] M. Boča, R. F. Jameson, W. Linert, *Coord. Chem. Rev.* **2011**, *255*, 290-317.
[20] J. Olguín, S. Brooker, *Coord. Chem. Rev.* **2011**, *255*, 203-240.
[21] M. A. Halcrow, *New J. Chem.* **2014**, *38*, 1868-1882.
[22] G. A. Craig, O. Roubeau, G. Aromi, *Coord. Chem. Rev.* **2014**, *269*, 13-31.
[23] M. A. Halcrow, *Coord. Chem. Rev.* **2009**, *253*, 2493-2514.
[24] M. Haryono, F. W. Heinemann, K. Petukhov, K. Gieb, P. Müller, A. Grohmann, *Eur. J. Inorg. Chem.* **2009**, *2009*, 2136-2143.
[25] D. Gentili, N. Demitri, B. Schaefer, F. Liscio, I. Bergenti, G. Ruani, M. Ruben, M. Cavallini, *J. Mater. Chem. C* **2015**, *3*, 7836-7844.
[26] B. Li, R.-J. Wei, J. Tao, R.-B. Huang, L.-S. Zheng, Z. Zheng, *J. Am. Chem. Soc.* **2010**, *132*, 1558-1566.
[27] J. Sanchez Costa, S. Rodriguez-Jimenez, G. A. Craig, B. Barth, C. M. Beavers, S. J. Teat, G. Aromi, *J. Am. Chem. Soc.* **2014**, *136*, 3869-3874.
[28] L. A. Barrios, C. Bartual-Murgui, E. Peyrecave-Lleixà, B. Le Guennic, S. J. Teat, O. Roubeau, G. Aromí, *Inorg. Chem.* **2016**, *55*, 4110-4116.
[29] M. Ohba, K. Yoneda, G. Agusti, M. Carmen Munoz, A. B. Gaspar, J. A. Real, M. Yamasaki, H. Ando, Y. Nakao, S. Sakaki, S. Kitagawa, *Angew. Chem. Int. Ed.* **2009**, *48*, 4767-4771.
[30] G. Aromi, C. M. Beavers, J. Sanchez Costa, G. A. Craig, G. Minguez Espallargas, A. Orera, O. Roubeau, *Chem. Sci.* **2016**, 10.1039/C1035SC04287A.
[31] D.-W. Tan, J.-B. Xie, Q. Li, H.-X. Li, J.-C. Li, H.-Y. Li, J.-P. Lang, *Dalton Trans.* **2014**, *43*, 14061-14071.
[32] M. Shatruk, H. Phan, B. A. Chrisostomo, A. Suleimenova, *Coord. Chem. Rev.* **2015**, *289–290*, 62-73.

[33] W. Jin, L. Wang, Z. Yu, *Organometallics* **2012**, *31*, 5664-5667.
[34] C.-M. Che, C.-F. Chow, M.-Y. Yuen, V. A. L. Roy, W. Lu, Y. Chen, S. S.-Y. Chui, N. Zhu, *Chem. Sci.* **2011**, *2*, 216-220.
[35] G. A. Craig, J. Sanchez Costa, O. Roubeau, S. J. Teat, G. Aromi, *Chem., Eur. J.* **2011**, *17*, 3120-3127.
[36] M. Sorai, S. Seki, *J. Phys. Chem. Solids* **1974**, *35*, 555-570.
[37] M. Sorai, Y. Nakazawa, N. Nakano, Y. Miyazaki, *Chem. Rev.* **2013**, *113*, PR41-PR122.
[38] Z. Arcis-Castíllo, S. Zheng, M. A. Siegler, O. Roubeau, S. Bedoui, S. Bonnet, *Chem. Eur. J.* **2011**, *17*, 14826-14836.
[39] O. Roubeau, M. Castro, R. Burriel, J. G. Haasnoot, J. Reedijk, *J. Phys. Chem. B* **2011**, *115*, 3003-3012.
[40] M. Sorai, *Top. Curr. Chem.* **2004**, *235*, 153-170.
[41] T. Nakamoto, Z. C. Tan, M. Sorai, *Inorg. Chem.* **2001**, *40*, 3805-3809.
[42] O. Roubeau, M. Evangelisti, E. Natividad, *Chem. Commun.* **2012**, *48*, 7604-7606.
[43] S. A. Barrett, C. A. Kilner, M. A. Halcrow, *Dalton Trans.* **2011**, *40*, 12021-12024.
[44] G. Lemercier, N. Brefuel, S. Shova, J. A. Wolny, F. Dahan, M. Verelst, H. Paulsen, A. X. Trautwein, J.-P. Tuchagues, *Chem., Eur. J.* **2006**, *12*, 7421-7432.
[45] M. Darawsheh, L. A. Barrios, O. Roubeau, S. J. Teat, G. Aromi, *Chem., Eur. J.* **2016**, *22*, 8635-8645.
[46] G. Lemercier, N. Bréfuel, S. Shova, J. A. Wolny, F. Dahan, M. Verelst, H. Paulsen, A. X. Trautwein, J.-P. Tuchagues, *Chem., Eur. J.* **2006**, *12*, 7421-7432.
[47] J. J. McKinnon, M. A. Spackman, A. S. Mitchell, *Acta Crystallogr., Sect. B* **2004**, *60*, 627-668.
[48] J. J. McKinnon, D. Jayatilaka, M. A. Spackman, *Chem. Commun.* **2007**, 3814-3816.
[49] M. A. Spackman, J. J. McKinnon, *CrystEngComm* **2002**, *4*, 378-392.
[50] *SAINT and SADABS*, Bruker AXS Inc., Madison, Wisconsin, USA.
[51] G. M. Sheldrick, *Acta Cryst. A* **2015**, *71*, 3-8.
[52] G. M. Sheldrick, *Acta Cryst. A* **2015**, *71*, 9-18.

FULL PAPER

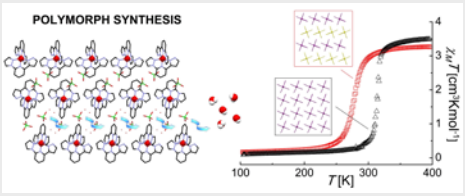

C. Bartual-Murgui, C. Codina, O. Roubeau* and G. Aromí**

Page No. – Page No.

A Sequential Method to Prepare Polymorphs and Solvatomorphs of $[Fe(1,3bpp)_2](ClO_4)_2 \cdot nH_2O$ (n=0,1,2) with Varying Spin Crossover Behavior

Two spin crossover (SCO) polymorphs, **1** and **2**, of an Fe(II) complex are prepared through a novel method; **1** is obtained directly from solution and **2** forms through single-crystal-to-single-crystal removal of water from the solvatomorph **2**·H_2O, obtained also pure. Polymorphs **1** and **2** exhibit distinct SCO properties.